Meteoritics & Planetary Science 33, 821–833 (1998)

Kamacite sulfurization in the solar nebula

D. S. LAURETTA[1,2]*, K. LODDERS[1] AND B. FEGLEY, JR.[1]

[1]Planetary Chemistry Laboratory, Department of Earth and Planetary Science, Campus Box 1169, Washington University, One Brookings Drive, St. Louis, Missouri 63130-4899, USA
[2]Present address: Arizona State University, Department of Geology, Tempe, Arizona 85287-1404, USA
*Correspondence author's e-mail address: dante.lauretta@asu.edu

(Received 1997 June 12; accepted in revised form 1997 December 23)
(Part of a series of papers dedicated to the memory of Paul Barringer)

Abstract–The kinetics and mechanisms of kamacite sulfurization were studied experimentally at temperatures and H_2S/H_2 ratios relevant to the solar nebula. Pieces of the Canyon Diablo meteorite were heated at 558 K, 613 K, and 643 K in 50 parts per million by volume (ppmv) H_2S-H_2 gas mixtures for up to one month. Optical microscopy and x-ray diffraction analyses show that the morphology and crystal orientation of the resulting sulfide layers vary with both time and temperature. Electron microprobe analyses reveal three distinct phases in the reaction products: monosulfide solid solution (mss), $(Fe,Ni,Co)_{1-x}S$, pentlandite $(Fe,Ni,Co)_{9-x}S_8$, and a P-rich phase. The bulk composition of the remnant metal was not significantly changed by sulfurization. Kamacite sulfurization at 558 K followed parabolic kinetics for the entire duration of the experiments. Sulfide layers that formed at 613 K grew linearly with time, while those that formed at 643 K initially grew linearly with time then switched to parabolic kinetics upon reaching a critical thickness. The experimental results suggest that a variety of thermodynamic, kinetic, and physical processes control the final composition and morphology of the sulfide layers. We combine morphological, x-ray diffraction, electron microprobe, and kinetic data to produce a comprehensive model of sulfide formation in the solar nebula. Then, we present a set of criteria to assist in the identification of solar nebula condensate sulfides in primitive meteorites.

INTRODUCTION

Iron, Ni, and S are three of the most abundant rock-forming elements in the solar system (Anders and Grevesse, 1989). As a result, metal and sulfide minerals are present in almost every type of chondrite. The distribution of these three elements among meteoritic minerals reflects their chemical and physical history. For example, the distribution of Fe between metal and silicates is one of the best indicators of meteorite oxidation states (Rubin *et al.*, 1988). The heterogeneity of Fe/Mg ratios in chondritic silicates is related to the extent of thermal metamorphism on their parent bodies (McSween *et al.*, 1988). The composition of chondritic metal grains records their parent body cooling rates (Herpfer *et al.*, 1994). The microstructure of Fe,Ni metal and sulfides in ordinary chondrites can be used to extract information about their postshock thermal histories (Bennett and McSween, 1996). Sulfides in CI chondrites, which contain some of the oldest Xe retention ages ever measured (Lewis and Anders, 1975), may preserve information about their formation in the solar nebula (Kerridge, 1977; Kerridge, 1979). In order to accurately interpret the information recorded in meteoritic metal and sulfides, the distribution of Fe, Ni, and S prior to parent body formation must be understood.

Much of our knowledge about the chemistry of the Fe-Ni-S system in the solar nebula results from thermodynamic equilibrium modeling. This approach uses solar elemental abundances and thermodynamic data to predict mineral stabilities as a function of nebular temperature and pressure (Grossman and Larimer, 1974; Lewis, 1972). These models predict that Fe, Ni, and S are in gaseous form at temperatures >1400 K. Direct condensation of Fe-rich metal grains occurs between 1200–1400 K, depending on the total pressure (Kelly and Larimer, 1977; Sears, 1978). The metal composition varies with temperature, with relatively Ni-rich metal condensing first. At these temperatures, P also has siderophile tendencies and condenses in solid solution with metal (Fegley and Lewis, 1980). When the siderophile elements are fully condensed, the solar-composition metal contains 93.8 wt% Fe, 5.4 wt% Ni, 0.3 wt% Co, and 0.6 wt% P (Anders and Grevesse, 1989).

Above 710 K, the dominant S-bearing species in the solar nebula is H_2S gas, which is present at the sulfur solar abundance of $S/H_2 = 33$ parts per million by volume (ppmv) (Anders and Grevesse, 1989; Dreibus *et al.*, 1995). Below 710 K, thermodynamic equilibrium calculations predict S condensation *via* the net thermochemical reaction:

$$\text{kamacite } (\alpha) + H_2S\ (g) \rightarrow \text{kamacite } (\alpha) + \text{taenite } (\gamma) + FeS + H_2\ (g) \qquad \text{Eq. (1)}$$

The mechanism of S condensation differs from that of the siderophile elements in that S condenses by a gas-solid reaction. Kerridge (1979) noted that sulfides in CI chondrites are inconsistent with Eq. (1) because they contain excess S and abundant Ni (*i.e.*, $(Fe,Ni)_{1-x}S$) compared to troilite (FeS). They suggested that thermodynamic equilibrium may have been inhibited during sulfide formation due to sluggish diffusion. Experimental sulfurization of Fe,Ni alloys can resolve this issue.

Several studies of Fe,Ni alloy sulfurization are reported in the metallurgical literature. These are summarized in Table 1 along with our experimental conditions and those for sulfide formation in the solar nebula. The previous studies were performed at conditions far removed from those of the solar nebula. Here we present the results of sulfide formation experiments designed to characterize the morphology and composition of primary nebular metal-sulfide assemblages. This study represents the first experimental investigation of Fe,Ni sulfurization at temperature and compositional conditions relevant to the solar nebula.

EXPERIMENTAL AND ANALYTICAL PROCEDURES

Our experiments are designed to simulate H_2S-H_2 ratios, temperatures, and alloy composition for sulfide formation in the solar nebula. The experimental procedure and apparatus are similar to

TABLE 1. Previous studies of iron-nickel sulfurization.

Reference	Ni content (wt%)	Gas	Temperature (K)	log f_{S2} (atm)
Strafford and Manifold, 1969	5	S_2	773	−3.9 to −1.9
Narita and Nishida, 1976*	2–15.2	S_2	833–1173	0
Skrzypek and Werber, 1976†	0.9–48.1	S_2	798–1098	0
Orchard and Young, 1989‡	41	H_2S-H_2-N_2	793–938	−9.7 to −5.2
This work	6.3	H_2S-H_2	558–643	−14.4 to −13.3
Solar Nebula	5.5	H_2S-H_2	400–710§	−18.0 to −13.0

*See also Narita and Nishida, 1975.
†See also Werber *et al.*, 1970.
‡See also Orchard and Young, 1989b; Young and Orchard, 1991.
§Temperature range from FeS stability through 100% S condensation (Lauretta *et al.*, 1996a).

that used in our previous study of iron sulfide formation from pure Fe metal (Lauretta *et al.*, 1996a). Polished, inclusion-free slabs of the Canyon Diablo (bulk composition, $Fe_{93.0}Ni_{6.3}Co_{0.5}P_{0.2}$) iron meteorite were heated at 558, 613, or 643 K in controlled atmospheres containing 50 ppmv H_2S, balance H_2 gas at ambient atmospheric pressure. The 50 ppmv H_2S gas mixture was produced by mixing 500 ppmv H_2S-H_2 gas with ultrahigh purity H_2 gas at a ratio of 1:9. The gas composition both before and after passing through the reaction chamber was measured with a Hewlett-Packard 5890 gas chromatograph calibrated against a suite of commercial certified H_2S-H_2 gas mixtures. Multiple experiments were done for varying times at each temperature to determine the variation in layer morphology, composition, and reaction progress. A complete list of the experimental conditions is given in Table 2.

After reaction, the sample weight gain was measured to determine the reaction progress. Optical microscopy provided information on sulfide layer morphologies and growth kinetics. X-ray diffraction (XRD) patterns of the sample surfaces were obtained using a Rigaku vertical powder diffractometer with Cu-Kα (λ = 1.540598 Å) radiation and Materials Data Incorporated software. The XRD patterns characterize sulfide orientation and mineralogy. Electron microprobe analyses were done with the Washington University JEOL-733 electron microprobe equipped with Advanced Microbeam automation. An accelerating voltage of 15 kV was used with 30 nA beam current and a beam diameter of 1 μm. X-ray matrix corrections were based on a modified Armstrong (1988) CITZAF routine. Pyrite (FeS_2) was used as the Fe and S standard, millerite (NiS) was used as the Ni standard, cobalt pentlandite (Co_9S_8) was used for Co, and gallium phosphide (GaP) was used for P. The electron microprobe analyses were used to measure spatial variations in the composition of the sulfide layers.

TABLE 2. Canyon Diablo sulfurization experiments in 50 ppm H_2S-H_2.

Run No.	Time (hours)	Initial Length (cm)	Initial Width (cm)	Initial Thick (cm)	Initial weight (g)	Final weight (g)	Sulfide Thickness (μm)	Wt. Gain/ unit area (g cm^{-2})
558 K								
CD 28	24.1	0.6652	0.4096	0.0401	0.081304	0.082706	21.3	2.22E-03
CD 16	70.7	0.8502	0.3693	0.0471	0.113336	0.117591	40.5	5.73E-03
CD 10	240.2	0.7871	0.3920	0.0730	0.176007	0.183687	83.2	9.73E-03
CD 13	359.8	0.8296	0.3818	0.0686	0.161967	0.171266	115.2	1.16E-02
CD 19	477.2	0.5935	0.4325	0.0457	0.087621	0.096759	125.9	1.51E-02
CD 22	544.4	0.5960	0.4230	0.0445	0.086399	0.095436	134.4	1.52E-02
CD 25	744.6	0.5177	0.4255	0.0465	0.076007	0.084306	NA	1.57E-02
613 K								
CD 29	24.1	0.5291	0.4299	0.0469	0.080516	0.080551	4.0	6.42E-05
CD 17	70.7	0.5799	0.4274	0.0410	0.075798	0.076391	12.0	1.03E-03
CD 11	240.2	0.8500	0.3837	0.0510	0.108557	0.109790	24.0	1.58E-03
CD 14	359.8	0.8400	0.3829	0.0512	0.122871	0.126943	50.7	5.05E-03
CD 20	477.2	0.6142	0.4246	0.0429	0.081899	0.084986	57.3	5.30E-03
CD 23	544.4	0.6545	0.4191	0.0459	0.094755	0.098970	70.0	6.51E-03
CD 26	744.6	0.5696	0.4261	0.0461	0.084477	0.089285	106.7	8.33E-03
643 K								
CD 30	24.1	0.6996	0.3962	0.0466	0.095077	0.095554	10.0	7.27E-04
CD 18	70.7	0.5390	0.4260	0.0392	0.067066	0.068733	16.0	3.12E-03
CD 12	240.2	0.8610	0.3756	0.0517	0.122390	0.125892	30.6	4.52E-03
CD 15	359.8	0.7534	0.4050	0.0320	0.070216	0.075653	58.3	7.94E-03
CD 21	477.2	0.7389	0.3743	0.0537	0.107650	0.114097	77.5	9.58E-03
CD 24	544.4	0.7430	0.3533	0.0344	0.066307	0.072913	118.0	1.10E-02
CD 27	744.6	0.5515	0.4293	0.0451	0.080407	0.087603	136.5	1.28E-02

NA = not analyzed.

EXPERIMENTAL RESULTS

Sulfide Microstructure and Morphology

The temporal variation of the sulfide layer morphologies provides information on their growth mechanisms. Figure 1 shows four optical, reflected light photomicrographs illustrating the growth sequence of sulfide layers on Canyon Diablo in 50 ppmv H_2S-H_2 gas at 558 K. Initially (Fig. 1a, 71 h), an outer layer of fine-grained monosulfide solid solution (mss) crystals and a thin, inner layer of P-bearing, Ni-rich grains form. Narrow, uniformly oriented mss crystals grow at the outermost edge of the sulfide layer at the expense of the fine-grained mss crystals (right side, Fig. 1a). Sulfide formation proceeds by the outward diffusion of cations, resulting in long, horizontal gaps between the metal and sulfide. As the reaction progresses (Fig. 1b, 240 h), the narrow mss crystals merge into a continuous, compact layer at the outer edge of the sulfide and small grains of pentlandite form between them. The long mss crystals also grow downward into the fine-grained portion of the outer layer. The brightness of the small mss grains decreases in regions near the narrow mss crystals due to increasing porosity. With further reaction progress (Fig. 1c, 360 h), the outer, compact mss-pentlandite layer gets thicker. The narrow mss crystals continue to grow downward, extending almost two-thirds of the way to the lower edge of the outer layer. The inner, P-rich layer becomes compact and a third, P-rich layer starts to form underneath it. After a very large extent of reaction (Fig. 1d, 544 h), the outer region of uniformly oriented mss grains becomes very thick. The narrow mss crystals consume most of the original, fine-grained mss layer. All that is left of this layer is a thin band along the lower edge of the outer layer. The third, innermost layer has grown as thick as the middle layer that lies above it.

Figure 2 shows a series of photomicrographs of sulfide layers that formed on Canyon Diablo in 50 ppmv H_2S-H_2 gas at 613 K. Though these samples reacted only 55° higher than those shown in Fig. 1, their morphology is strikingly different. Initially, a very porous, mss layer containing evenly dispersed pentlandite inclusions forms (Fig. 2a, 71 h). Several small, P-rich crystals form concurrently in the gap that separates the outer mss layer from the metal. With a larger extent of reaction (Fig. 2b, 240 h), the mss-pentlandite layer grows thicker but its overall morphology does not change. The small, P-rich crystals begin to merge together and form a second, inner layer. As the reaction continues (Fig. 2c, 360 h), the outer layer obtains a uniform width. Abundant pores and small pentlandite grains are evenly distributed throughout the outer layer.

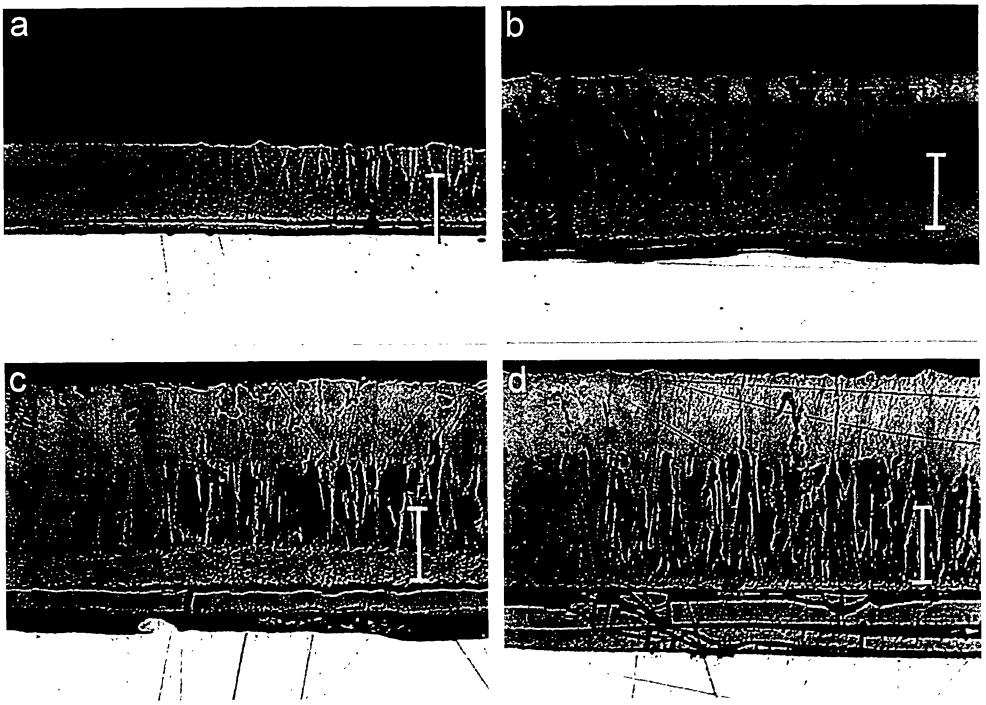

FIG. 1. A series of reflected light photomicrographs illustrating the growth of sulfide layers on Canyon Diablo in 50 ppm H_2S-H_2 at 558 K. In all photos, the remnant metal lies along the bottom edge. Scale bar in all photos = 32 μm. (a) Sample CD16 reacted for 71 h. Two sulfide layers are present. The inner layer is composed of P-rich sulfides. The outer layer contains fine-grained mss crystals that are being consumed by uniformly oriented mss crystals (top right). (b) Sample CD10 reacted for 240 h. The outer portion of the layer is composed of mss (dark gray) and pentlandite (light gray) crystal. The color variation in the fine-grained portion of the outer layer is due to increasing porosity. (c) Sample CD 13 reacted for 360 h. The compact portion now comprises almost one-third of the outer layer. The P-rich, inner layer has become compact. A third, innermost layer has started to form. (d) Sample CD19 reacted for 477 h. Three distinct layers are present. The fine-grained portion of the outer layer has been almost entirely consumed.

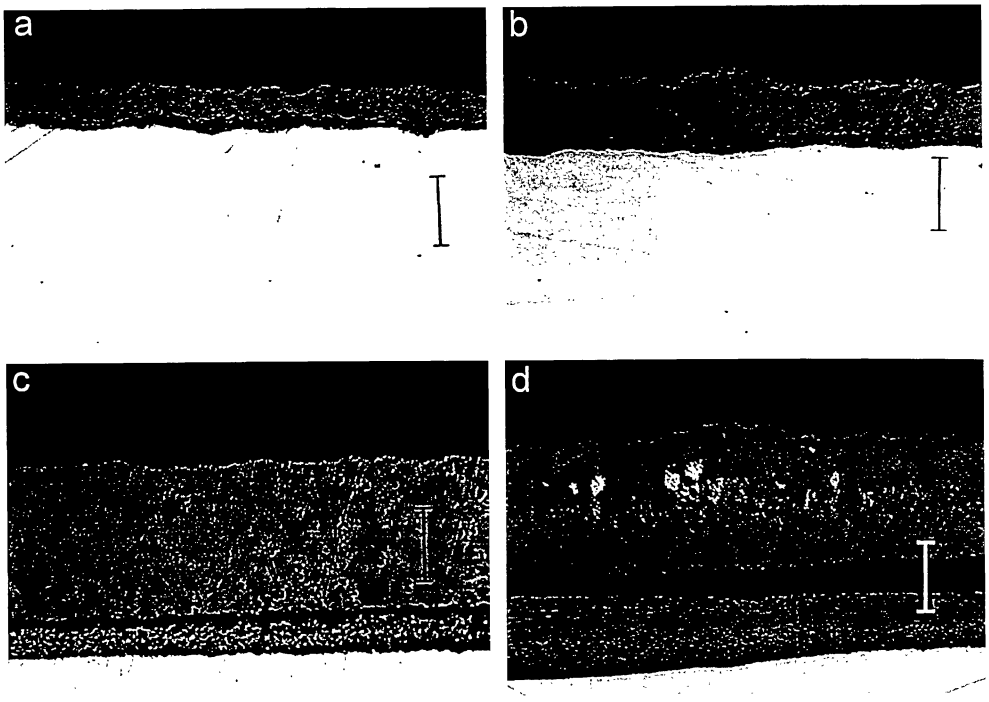

FIG. 2. A series of reflected light photomicrographs illustrating the growth of sulfide layers on Canyon Diablo in 50 ppm H_2S-H_2 at 613 K. In all photos, the remnant metal lies along the bottom edge. Scale bar in a–c = 20 μm, d = 32 μm. (a) Sample CD17 reacted for 71 h. The outer layer is composed of fine-grained mss and pentlandite crystals. A few P-rich sulfide grains are present in the gap between metal and sulfide. (b) Sample CD11 reacted for 240 h. The sulfide morphology is similar to that in (a) only larger. The P-rich sulfides are slightly more abundant. (c) Sample CD 14 reacted for 360 h. Two sulfide layers are now clearly visible. Both are fine-grained and porous. (d) Sample CD26 reacted for 745 h. The outer layer is compact, and the pentlandite inclusions have concentrated in the center of the layer.

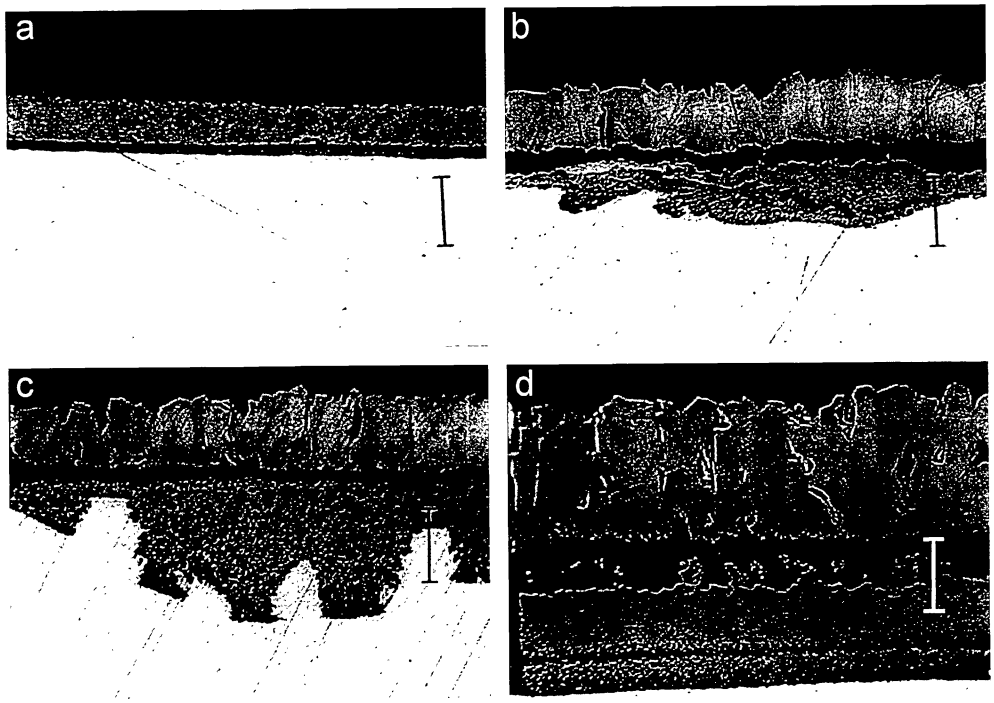

FIG. 3. A series of reflected light photomicrographs illustrating the growth of sulfide layers on Canyon Diablo in 50 ppm H_2S-H_2 at 643 K. In all photos, the remnant metal lies along the bottom edge. Scale bar in all photos = 32 μm. (a) Sample CD18 reacted for 71 h. The outer layer is composed of fine-grained mss and pentlandite crystals. A few P-rich sulfide grains are present in the gap between metal and sulfide. (b) Sample CD15 reacted for 360 h. The outer layer now contains uniformly oriented crystals. The inner layer has selectively consumed an initially Ni-rich region of the metal. (c) Sample CD21 reacted for 477 h. Outer layer morphology is unchanged. Kamacite protrudes into the inner layer. (d) Sample CD27 reacted for 745 h. The outer layer is compact and the inner layer has reached a uniform width.

The fine-grained P-rich crystals become abundant enough to form a very porous, inner layer. With a large extent of reaction (Fig. 2d, 745 h), the morphology of the outer layer changes. The mss crystals develop a uniform orientation and the overall porosity decreases with only occasional large pores present. The pentlandite inclusions grow larger and concentrate in the center of the outer layer. The inner layer becomes quite extensive. It is still fine-grained and porous but a compact region forms in its center.

Figure 3 shows the growth sequence of sulfide layers that formed on Canyon Diablo in 50 ppmv H_2S-H_2 gas at 643 K. The morphology is similar to that of the samples shown in Fig. 2. However, there are several interesting distinctions. Initially (Fig. 3a, 71 h), a porous layer forms, which contains fine-grained mss crystals and small pentlandite grains. Several very small crystals of a P-rich phase also form in the void space that separates metal from sulfide. With further reaction (Fig. 3b, 360 h), the mss crystals of the outer layer develop a uniform orientation and the overall porosity decreases. The inner, P-rich layer preferentially consumes initially Ni-rich regions of the metal leaving the metal sulfide interface rough and distorted. As the reaction progresses (Fig. 3c, 477 h), the outer sulfide layer gets larger. The inner layer continues to consume regions of Ni-rich metal, leaving behind pillars of kamacite. After a very large extent of reaction (Fig. 3d, 745 h), the outer layer gets thicker without significant morphological change. The thickness of the inner layer evens out. A third, porous layer forms next to the metal.

Despite the large variation in the microstructure and morphology of the sulfide layers, they all contain similar features. Eventually, all the samples develop a multilayer structure. Typically, there is at least one porous, inner layer containing a fine-grained P-rich phase. Initially, the outer layers are composed of fine-grained, randomly oriented mss crystals. As the reaction progresses, uniformly oriented mss crystals and pentlandite grains consume the fine-grained portion of the outer layer. Long, horizontal gaps, created by outward cation diffusion, separate the sulfide layers from each other and from the metal. The sulfide growth sequences will be used in conjunction with the structural, compositional, and kinetic data presented in the next three sections to provide a picture of sulfide formation mechanisms.

X-ray Diffraction Results

X-ray diffraction (XRD) patterns of the sample surfaces provide information on the composition, structure, and orientation of the outermost portion of the sulfide layer as a function of time (Fig. 4). Three phases were detected in the XRD analyses: α-mss (*i.e.*, structurally similar to α-FeS, which has a distorted NiAs structure), pentlandite, and kamacite. The locations of the highest intensity reflections from each of these phases are labeled at the top of Fig. 4 along with their corresponding Miller indices. Figure 4a–c shows the XRD patterns of three sulfide layers that formed at 558 K. The XRD pattern from the sample that reacted for 24 h (Fig. 4a) contains high-intensity peaks at 30° and 53° (all angles refer to values of 2θ). This suggests that mss crystals at the outer edge of this sample are predominantly oriented along the (110) and (300) planes of the mss unit cell. The presence of a small reflection at 51° corresponding to the pentlandite (440) plane indicates that a small amount of pentlandite is also present in this sulfide layer. After longer reaction times (360 and 745 h, Fig. 4b–c), the mss reflection at 53° dominates the XRD patterns, indicating that mss crystals oriented along (300) have outgrown crystals with other orientations.

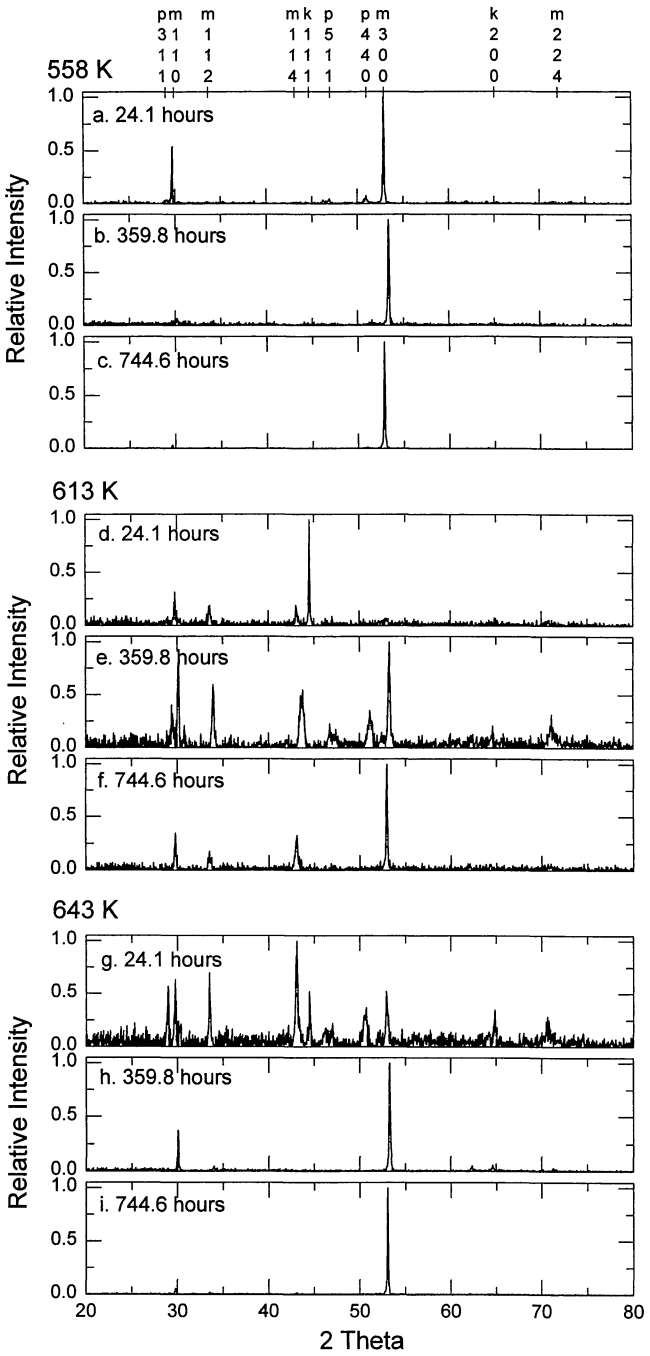

FIG. 4. Graphs showing relative intensity x-ray diffraction patterns of the surfaces of our experimental samples. The locations of high-intensity reflections from mss (m), pentlandite (p), and kamacite (k) planes are indicated at the top. A single, high-intensity peak corresponds to a uniform orientation in the mss crystals, while abundant smaller peaks imply random orientations.

The XRD patterns obtained from surfaces of samples that reacted at 613 K are shown in Fig. 4d–f. A high-intensity reflection at 45°, corresponding to the (111) plane of kamacite, dominates the XRD pattern in Fig. 4d (24 h). This implies that the sulfide layers on this sample are thin and do not obscure the underlying metal. Less intense peaks at 30°, 34°, and 44° suggest the existence of a thin mss layer. Many mss peaks (30°, 34°, 44°, 53°, and 72°) are present in the XRD pattern in Fig. 4e (360 h), which suggests that abundant, randomly oriented mss crystals are present. There are also relatively strong signals at 29° and 51° from pentlandite crystals. The mss reflection at 53° dominates the XRD pattern in Fig. 4f (745 h), which implies that the mss grains in this sample have begun to develop a preferred orientation.

Figure 4g–i shows the XRD patterns obtained from samples that formed at 643 K in 50 ppmv H_2S. The kamacite reflection at 45° is clearly visible in Fig. 4g (24 h), which indicates that the sulfide layers on this sample are still fairly thin. The presence of a variety of peaks (30°, 34°, 44°, 53° and 72°) in Fig. 4g is consistent with the XRD pattern of abundant, randomly oriented mss crystals. Relatively high intensity peaks are present at 29° and 51°, which indicates the presence of pentlandite. The XRD pattern in Fig. 4h (360 h) is dominated by two mss peaks at 30° and 53°. This is similar to the pattern in Fig. 4a and suggests that the mss crystals at the outer edge of this sample are predominantly oriented with their (110) and (300) planes parallel to the metal surface. The XRD pattern in Fig. 4i (745 h) is completely dominated by the mss reflection at 53°. This indicates that all mss crystals in this layer are uniformly oriented with their *a* axes perpendicular to the metal.

Comparison of the XRD patterns in Fig. 4 shows a significant variation in the development of the sulfide layers with temperature. The mss crystals that formed at 558 K quickly developed preferred orientations. This correlates with the sulfide layer morphologies shown in Fig. 1, in which the long, narrow mss crystals appear after very short reaction times. The mss crystals in the sulfide layers that formed at 613 K and 643 K were initially randomly oriented. A preferred orientation developed in the sulfide layers that formed at 613 K only after a very long reaction time (745 h). On the other hand, the sulfide crystals that formed at 643 K developed uniform orientations after 360 h of reaction. As will be discussed later, this is related to sulfide phase stabilities and reaction mechanisms.

Electron Microprobe Results

Electron microprobe traverses from the metal core to the outer edge of the sulfide layers to provide information on the compositional and mineralogical variation of the experimental samples. The results of three electron microprobe traverses are plotted in Figs. 5–7. Data from each traverse are reported in four different graphs. In each graph, distance is plotted on the *x* axis with zero corresponding to the metal-sulfide interface. The locations of the metal, inner layer, and outer sulfide layer are labeled at the top of each Figure. The *y* axes of the four different graphs correspond to cation/S atom ratios (Fe + Ni + Co/S), atomic Ni cation% (Ni/Fe + Ni + Co), atomic Co cation% (Co/Fe + Ni + Co), and atomic% P, (P/Fe + Ni + Co + S + P). These four variables completely characterize the composition of both metal and sulfide phases.

The cation/S ratio is used to identify different sulfide phases. There are two distinct sulfide phases present in our experimental samples. Monosulfide solid solution is the most abundant phase and has cation/S ratios ≤1. Values <1 correspond to deviations from ideal stoichiometry (1–x) as given in the formula $(Fe,Ni,Co)_{1-x}S$. Pentlandite, the other sulfide phase produced in our experiments, has an ideal cation/S ratio of 1.125. Deviations from this value are observed in both the experimental and natural samples (*e.g.*, Shewman and Clark, 1970). The inner layer that formed in our experiments contains abundant Ni and P and also has high cation/S ratios. The composition of the P-rich inner layer suggests that it may be composed of a fine-grained mixture of barringerite ($(Fe,Ni,Co)_2P$) and

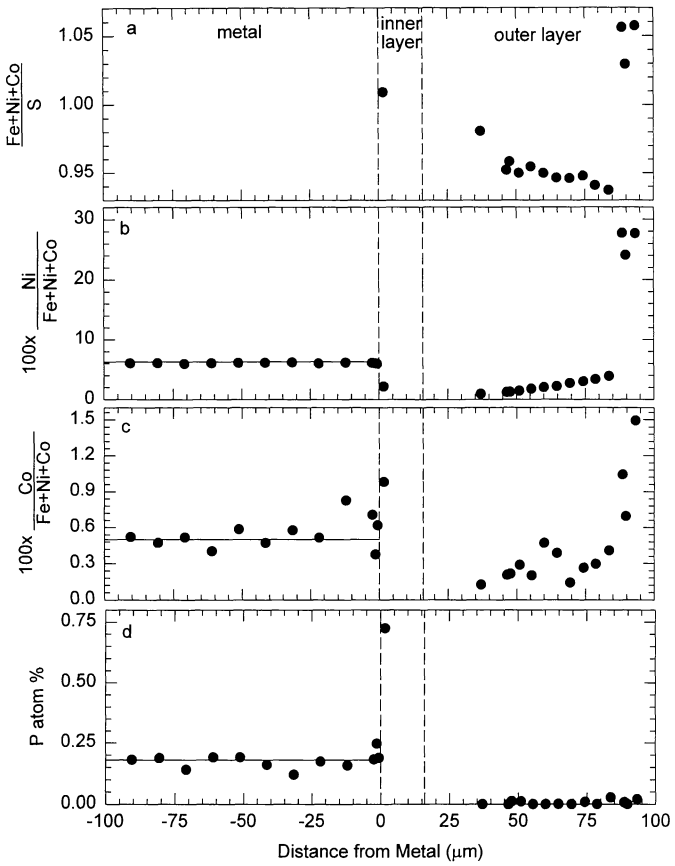

FIG. 5. Compositional variation of sample CD13 (558 K, 360 h). Distance is plotted on the x axis with zero corresponding to the metal-sulfide interface. The boundaries between the metal-inner sulfide layer and the inner-outer sulfide layers are indicated by dashed, vertical lines. The initial composition of the metal is given by the solid, horizontal lines. (a) Cation/S ratio. (b) Ni cation%. (c) Co cation%. (d) P atom%.

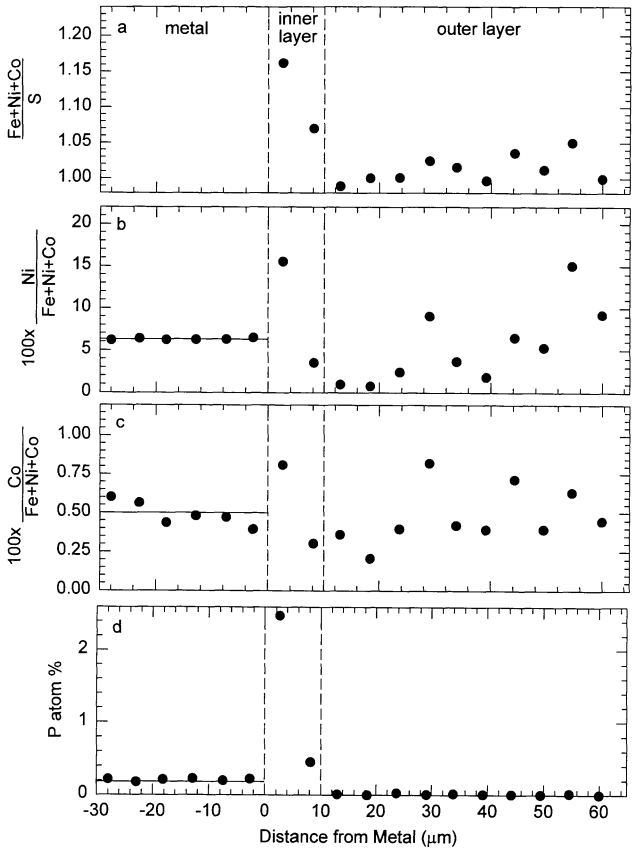

FIG. 6. Compositional variation of sample CD14 (360 h, 613 K). (See caption, Fig. 5).

mss ($(Fe,Ni,Co)_{1-x}S$). However, definitive identification of the phases in this layer requires higher resolution than that obtained with the electron microprobe.

The Ni and Co concentrations are reported as cation% to facilitate direct comparison of metal and sulfide compositions. The initial metal composition is indicated in Figs. 5–7 by solid, horizontal lines. The sulfide layers that formed in these experiments contain significant amounts of Ni and Co. By plotting the data as cation%, we can determine to what extent (if any) Ni and Co fractionate during sulfide formation.

Figure 5 shows the data from a microprobe traverse of a sample that sulfurized at 558 K in 50 ppmv H_2S for 360 h. There is no significant variation in the metal composition with distance from the metal-sulfide interface (Fig. 5b–d). The Ni and P contents of the remnant metal are indistinguishable from the initial composition. The Co content of the remnant metal varies, but the average value is the same as the starting composition. Only one analysis of the inner layer was obtained. The inner layer has a cation/S ratio of 1.01, contains 2.2 cation% Ni, 1.0 cation% Co, and 0.8 atom% P. The analyses 5–40 μm away from the metal in the fine-grained portion of the outer layer all yielded low totals, which were likely due to the high porosity of this region (see Fig. 1c). However, the elemental ratios of these analyses are consistent with mss. The cation/S ratio (Fig. 5a) in the compact portion of the outer layer decreases monotonically from 0.98 to 0.94 over a distance of 50 μm. The Ni content of this region (Fig. 5b) is inversely correlated with the cation/S ratio and increases from 1 to 5 cation% Ni. No P was detected in the outer layer (Fig. 5d). The high cation/S ratios, Ni, and Co cation% in the last 15 μm of the sulfide layer correspond to a mixture of mss and pentlandite grains.

The compositional variation of a metal-sulfide assemblage that formed after 360 h of reaction at 613 K is plotted in Fig. 6. Again, there is no significant variation in the metal composition, which has Ni, Co, and P concentrations virtually identical to those of the initial metal. The inner layer in this sample is thin (~10 μm) and only two analyses could be obtained. The inner layer contains as much as 2.6 atomic% P (Fig. 6d) and this large P content correlates with a high cation/S ratio. The P content decreases in the inner layer with distance from the metal surface and the outer layer is devoid of P. The cation/S ratios (Fig. 6a) of the outer layer oscillate between 0.99 and 1.05. The Ni and Co (Fig. 6b–c) contents correlate directly with the cation/S ratios. This indicates that submicron-sized grains of pentlandite are evenly dispersed throughout the outer mss layer.

The microprobe data plotted in Fig. 7 were obtained from an experimental sample reacted for 360 h at 643 K. The inner layer penetrates deeply into the metal (see Fig. 3c). The composition of this inner layer provides a clue to the formation mechanism of the P-rich phase. The metal in contact with the inner layer is enriched in both Ni (Fig. 7b) and P (Fig. 7d) (30 cation% and 1 atom%, respectively) and depleted in Co (Fig. 7c) (0.25 cation%) compared to the original bulk composition of the metal (solid lines, 6.3% Ni, 0.5% Co, 0.2% P). This is a region of taenite that extends an addi-

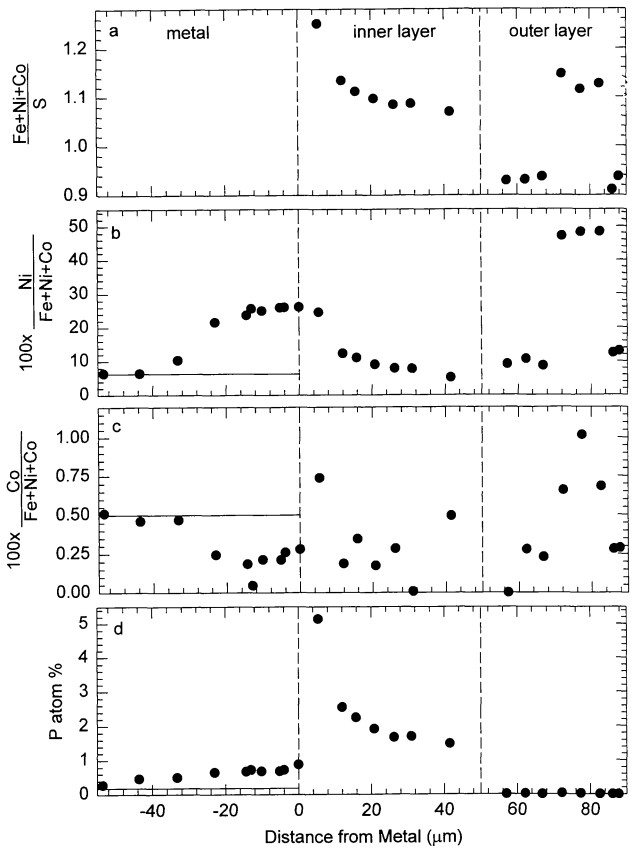

FIG. 7. Compositional variation of sample CD15 (360 h, 643 K). (See caption, Fig. 5).

tional ~40 μm from the interface indicating that it was present in the metal prior to sulfurization. The inner layer is >50 μm thick, has very high cation/S ratios, and is enriched in Ni and P. Thus, it appears that sulfurization of taenite produced the P-rich inner layer. The cation/S ratio (Fig. 7a) and the concentration of Ni (Fig. 7b) and P (Fig. 7d) decrease monotonically in the inner layer with distance from the metal. The outer sulfide layer of this sample is composed of P-free mss with cation/S ratios of ~0.92. A large pentlandite grain, which contains ~50 cation% Ni and 1 cation% Co, is present in the center of the outer layer.

Figure 8 shows three plots of measured compositional variation of our experimental sulfide layers at 558 K (Fig. 8a), 613 K (Fig. 8b), and 643 K (Fig. 8c). The data shown in Fig. 8 were obtained from electron microprobe traverses of every experimental sample. Figure 8a shows the compositional variation of the sulfide layers that formed at 558 K. The metal contains ~6 cation% Ni, which is identical to the starting composition. The composition of the P-rich phase extends from the lower edge of the mss field down to very S-depleted values. The composition of the outer sulfide layer extends between Ni-poor mss and pentlandite. A similar variation is seen in the samples that formed at 613 K (Fig. 8b). The Ni content of the metal is identical to that of the initial composition (6.3 cation% Ni). The P-rich phase has a variable composition that ends near the mss field. The outer layer contains mss with varying Ni content and pentlandite. The data plotted in Fig. 8c correspond to the sulfide layers that formed at 643 K. The composition of the taenite grain found in sample CD15 (see Fig. 7) plots between 20–30 cation% Ni. The high Ni-content of the P-rich phase corresponds to sulfurization

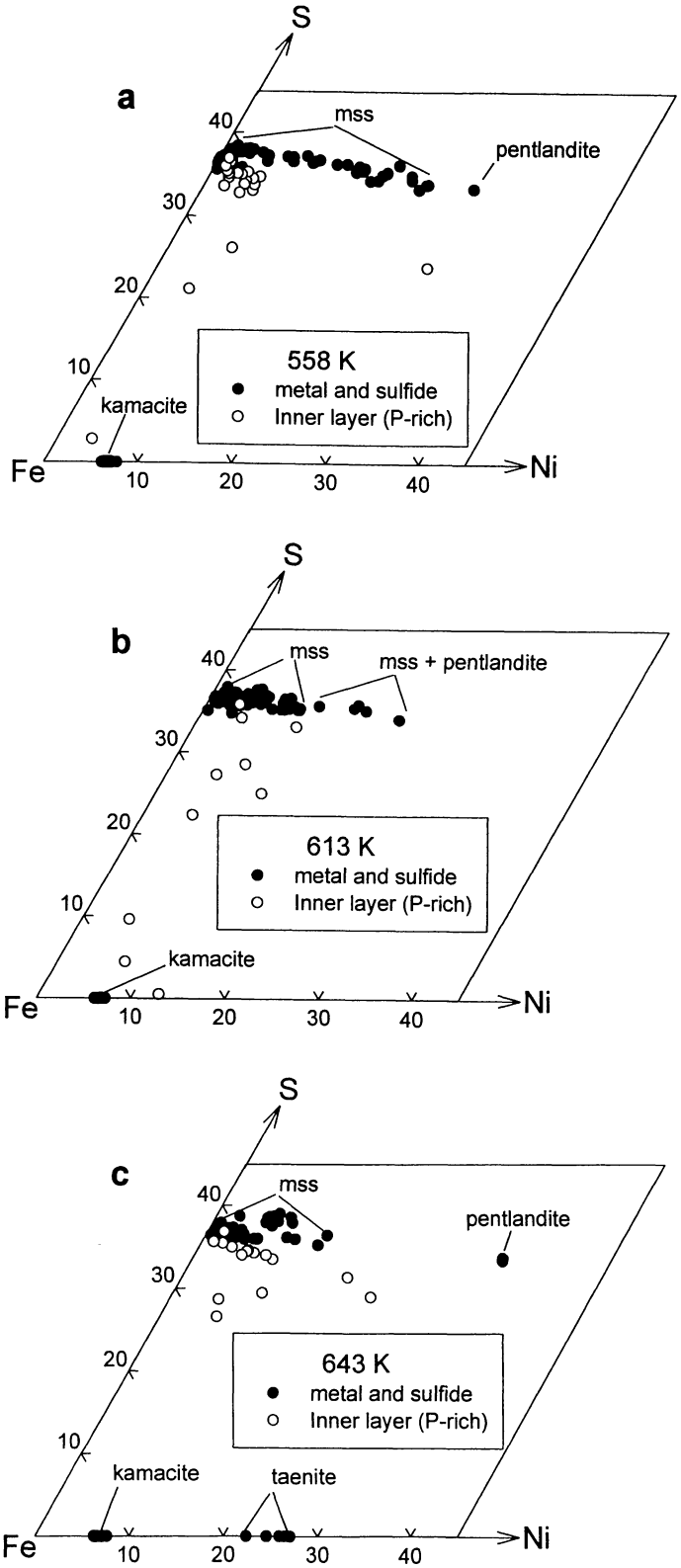

FIG. 8. Plots of the compositional variation of all experimental samples on Fe-Ni-S ternary phase diagrams (wt%). Solid circles indicate metal and sulfide compositions, while the open circles correspond the normalized Fe, Ni, and S contents of the P-rich phase. (a) 558 K. (b) 613 K. (c) 643 K.

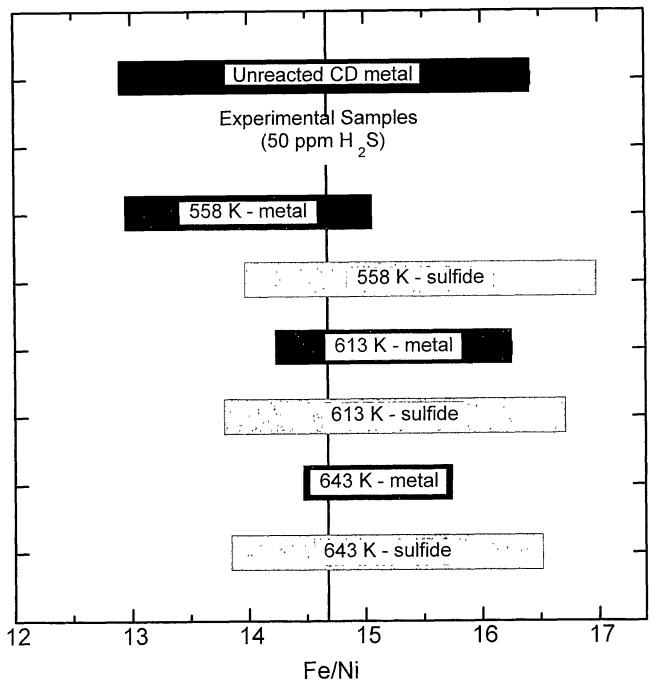

FIG. 9. A graph comparing the atomic Fe/Ni in the starting Canyon Diablo metal and the metal and sulfide phases after reaction. Data were collected using the Washington University electron microprobe with a variable beam size between 10–20 μm. Typically, ten spots were collected on the metal and sulfide from each sample. The vertical line shows the average starting metal composition. The range of each Fe/Ni ratio is 2σ of the mean value. Sulfurization does not significantly alter the composition of the metal. Instead, Ni is distributed equally between the metal and sulfide.

of taenite. The Ni content of the outer layer varies within the mss and extends out to pentlandite.

The microprobe data show that there is a large spatial variation in the composition of the sulfide layers. At each temperature studied, a Ni- and P-rich layer formed. This layer grew rapidly into regions of the metal that were initially rich in Ni and P (taenite grains). In most regions of the samples, the metal composition is equal to its initial composition. The outer sulfide layers are composed of mss with pentlandite inclusions. Usually, the S and Ni contents of the mss layer increase with distance from the metal. The presence of Ni and S concentration gradients is common in sulfide layers that form on binary alloys. Several other studies of Fe,Ni sulfurization report similar gradients in the resulting sulfide layers (Narita and Nishida, 1975; Orchard and Young, 1989a,b; Young and Orchard, 1991). There is a direct correlation between the Ni and Co contents in pentlandite.

Broad electron beam analyses were used on the metal and sulfide to determine their bulk Fe/Ni ratio. The results of these analyses are shown in Fig. 9. The bars in Fig. 9 correspond to the average bulk Fe/Ni atomic ratios and 2σ uncertainties for unreacted metal, partially reacted metal, and product sulfide layers. At all temperatures studied (558 K–643 K) our data show that the bulk Fe/Ni ratio is the same in both metal and sulfide. Sulfurization does not significantly fractionate Fe and Ni.

Reaction Kinetics

The rate of Canyon Diablo metal sulfurization in 50 ppmv H_2S was measured at 558, 613, and 643 K. Two methods were used to determine the reaction progress. In the gravimetric method, the extent of reaction was obtained by measuring the weight gain of samples that reacted for varying time periods. In the geometric method, the reaction progress was determined by measuring the variation in sulfide layer thickness with time. There is excellent agreement between the two methods. All kinetic data from this study are listed in Table 2. The gravimetric kinetic data are plotted in Fig. 10 as weight gain per unit area *vs.* reaction time, and our derived practical tarnishing rate constants are presented in Table 3. In addition, we determined the change in sulfide layer thickness as a function of time using the geometric data presented in Table 2. The equations describing this variation are:

558 K $\quad l = 5.7(\pm0.1) \times t^{1/2} - 0\ (\pm5) \quad r^2 = 0.993$ Eq. (2)

613 K $\quad l = 0.13(\pm0.01) \times t - 0\ (\pm5) \quad r^2 = 0.982$ Eq. (3)

643 K $\quad l = 0.15(\pm0.01) \times t - 0\ (\pm6) \quad r^2 = 0.961 \quad (t \leq 360)$ Eq. (4a)

643 K $\quad l = 9.9(\pm2.3) \times t^{1/2} - 128\ (\pm14) \quad r^2 = 0.904 \quad (t \geq 360)$ Eq. (4b)

where l is the sulfide layer thickness in micrometers, t is the reaction time in hours, and r^2 is the regression coefficient for each equation. The 1σ uncertainties are given in parentheses.

Both the gravimetric and geometric kinetic data indicate a change in the sulfurization kinetics between 558 K and 613 K. The sulfide layers grow most quickly at 558 K, the lowest temperature studied. In addition, the reaction progress at 558 K is proportional to the square root of the reaction time (parabolic kinetic behavior), while the reaction progress at 613 and 643 K is initially proportional to the reaction time (linear kinetic behavior). The linear reaction rate increases from 613 to 643 K. There is a transition from linear to parabolic kinetics at 643 K between 240 and 360 h of reaction.

The kinetic behavior correlates with the observed variation in sulfide orientation (Fig. 4). The sulfide layers formed at 558 K are uniformly oriented after very short reaction times. The growth of these layers followed parabolic kinetics throughout the entire reaction period. The sulfide layers formed at 613 K did not develop uniform orientations and sulfide growth followed linear kinetic behavior throughout the entire course of reaction. The sulfide layers formed at 643 K developed a uniform orientation after ~360 h of reaction. This switch to a preferred orientation correlates with the transition in the rate-controlling mechanism from H_2S dissociation (linear kinetics) to cation diffusion through the sulfide layer (parabolic kinetics). This relationship will be discussed in more detail in the next section.

The effect of Ni on the sulfurization rate of Fe,Ni alloys varies depending on the reaction conditions. Studies of Fe,Ni alloy sulfurization in pure S_2 vapor suggest that Ni-bearing metal sulfurizes at rates similar to those of pure Fe (Narita and Nishida, 1975; Skrzypek and Werber, 1976). However, Orchard and Young (1989a,b) and Young and Orchard (1991) found that Ni-bearing alloys sulfurize more rapidly than pure iron in H_2-H_2S-N_2 gas mixtures. They suggest that Ni-bearing sulfides catalyze H_2S dissociation resulting in increased S activities on the sulfide surfaces. Fryt *et al.*, (1979) found that the rate of pure Fe sulfurization is proportional to the square root of the S fugacity. The available data for Fe,Ni sulfurization do not reveal such a dependence (Orchard and Young, 1989a; Strafford and Manifold, 1969). However, the range of S fugacities studied to date is limited and more work needs to be done to quantify the effect of S fugacity on the rate of Fe,Ni sulfurization.

The rate constants for kamacite sulfurization determined in this study are compared to those of pure Fe in Table 4 (Lauretta *et al.*,

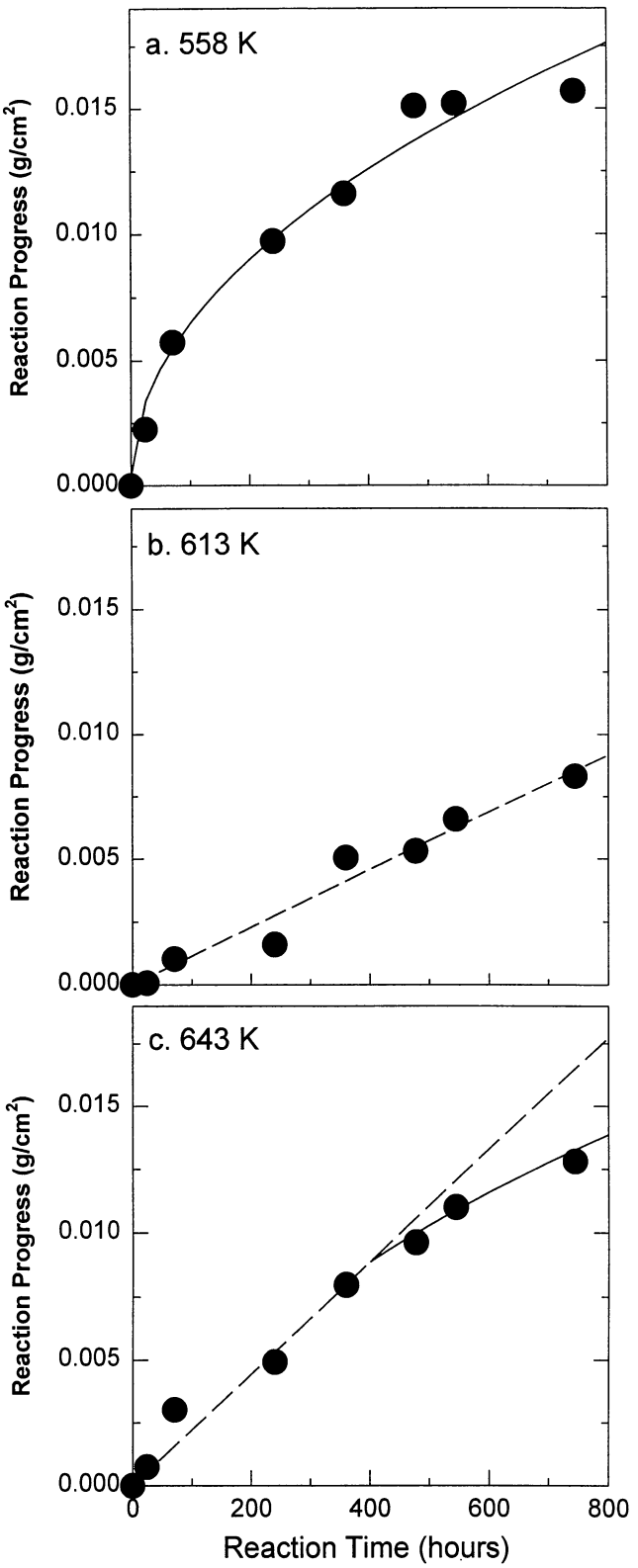

FIG. 10. Plots of the reaction progress at three different temperatures *vs.* time. Solid curves indicate regions of parabolic kinetic behavior, while dashed lines indicate linear kinetics. The samples at 558 K sulfurized rapidly and followed parabolic kinetics for the entire duration of the experiments. Sulfurization proceeded linearly at 613 K, while a transition from linear to parabolic kinetics occurred after 360 h of reaction at 643 K.

1996a). The rate of Fe sulfurization in 50 ppm H_2S followed linear kinetics at all temperatures studied. The rate constants for kamacite sulfurization at 613 K and 643 K are directly comparable to those for pure Fe. However at 558 K, kamacite sulfurization followed parabolic kinetics. As a result, a linear rate constant was not obtained and a direct comparison to the pure Fe data can not be made. We can infer that the rate of H_2S dissociation at 558 K is more rapid than the observed reaction rate, which therefore defines a lower limit. Kamacite sulfurization is faster than that of Fe metal by a factor of 24 at 643 K and at least 14 at 558 K. The two rates are identical at 613 K. The increase in reaction rate at 558 K may be due to the high Ni content at the outer edges of these sulfide layers (see next section). The similarity in the reaction rates at 613 K implies that the rate-limiting mechanism is the same in both cases. Finally at 643 K, the sulfide layers that formed on pure Fe developed a preferred orientation along their *c* axes, while those that formed at 613 K were preferentially oriented along their *a* axes. This change in orientation is likely responsible for the drop in reaction rate between these two temperatures. A corresponding switch in crystal orientation did not occur on the sulfide layers that formed at 643 K on kamacite. These layers are also oriented along their *a* axes, and therefore sulfurize at a rate comparable to that seen at 613 K. Additional experiments are needed to determine if the change in crystal orientation occurs at higher temperatures in the Fe-Ni-S system.

CHEMICAL AND PHYSICAL MECHANISMS OF SULFIDE FORMATION

The compositional and morphological variation of sulfide layers that form on meteoritic metal results from a series of physical and chemical mechanisms. Our model for metal sulfurization in a solar composition gas is qualitatively outlined in Fig. 11. The reaction begins when kamacite in contact with H_2S gas cools below 710 K and FeS becomes thermodynamically stable (Lauretta *et al.*, 1996a). A fraction of the H_2S gas molecules that collide with the metal become physically adsorbed on its surface. This is expressed by the reaction:

$$H_2S\ (g) + \square_m \rightarrow H_2S\ (ad_m) \qquad \text{Eq. (5)}$$

where $\square_m$ is a vacant metal surface site and (ad_m) refers to an adsorbed species on the metal surface. The rate of physical adsorption is inversely proportional to temperature (Kreuzer and Gortel, 1986).

TABLE 3. Sulfurization rate constants.

Temperature (K)	Kinetic Behavior	Practical Tarnishing Rate Constant ($\pm 1\sigma$)
558	Parabolic	$(3.4 \pm 0.1)10^{-7}$ g^2 cm^{-4} hr^{-1}
613	Linear*	$(1.2 \pm 0.1)10^{-5}$ g cm^{-2} hr^{-1}
643	Linear†	$(2.0 \pm 0.3)10^{-5}$ g cm^{-2} hr^{-1}
643	Parabolic	$(2.7 \pm 0.2)10^{-7}$ g^2 cm^{-4} hr^{-1}

*Transition thickness >107 μm.
†Transition thickness = 60 ± 15 μm.

TABLE 4. Kamacite *vs.* pure iron sulfurization kinetics.

Temperature (K)	Linear Rate Constant α	Linear Rate Constant Fe	Ratio α/Fe
558	$(>9.3)10^{-5}$	$(6.8)10^{-6}$	>13.7
613	$(1.2)10^{-5}$	$(1.2)10^{-5}$	1
643	$(2.0)10^{-5}$	$(8.3)10^{-7}$	24.1

This plausibly explains the observed decrease in reaction rate between 558 K and 613 K. However, if this is the rate-controlling mechanism in our experiments, then the reaction rate should also decrease between 613 K and 643 K, which is not observed. At the relatively low temperatures where sulfides are stable, there will be almost full coverage of the metal surface (Kreuzer and Gortel, 1986). Thus, the physical adsorption of gas molecules does not appear to be a rate-limiting mechanism.

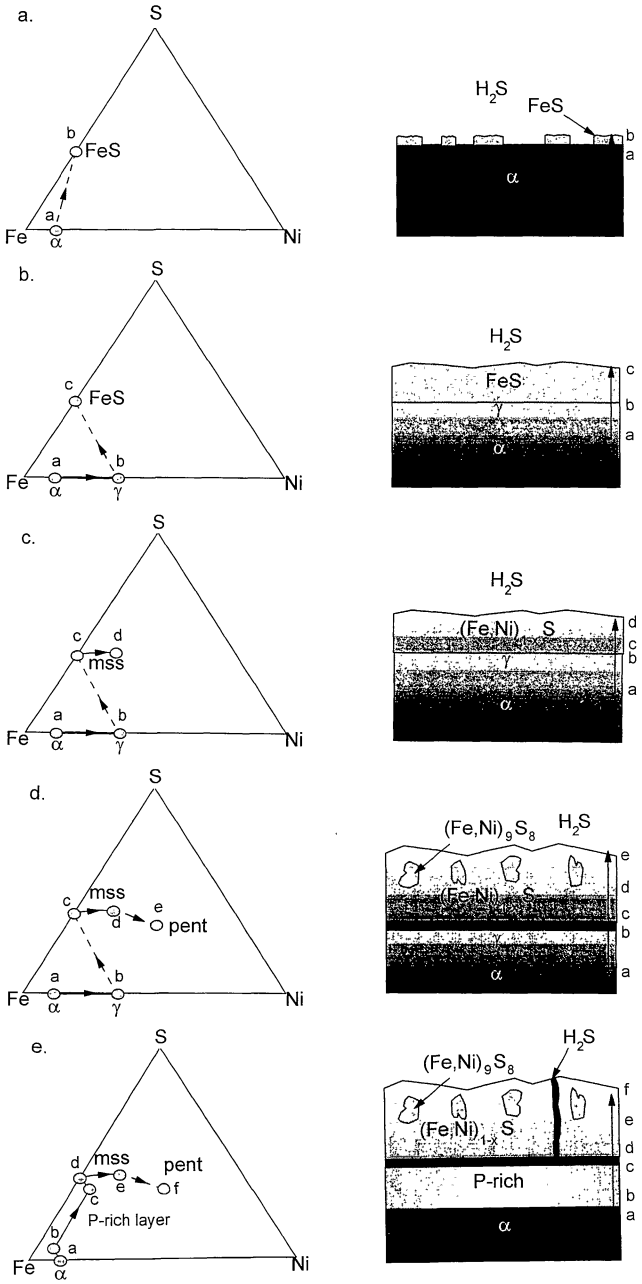

FIG. 11. A qualitative model of the physical and chemical processes that influence sulfide layer morphologies. The ternary plots illustrate the evolution of the diffusion path followed for kamacite sulfurization. The solid lines indicate a continual variation in composition. The dashed lines indicate equilibrium across an interface. The final predicted assemblage is a kamacite core surrounded by multiple sulfide phases. No net change in the metal composition occurs.

Instead at the initial stage of reaction, the rate-limiting mechanism is the dissociation of H_2S on the metal surface. The H_2S molecules dissociate through a series of reactions such as:

$$H_2S\,(ad_m) + \square_m \rightarrow HS\,(ad_m) + H\,(ad_m) \qquad \text{Eq. (6)}$$

$$HS\,(ad_m) + \square_m \rightarrow S\,(ad_m) + H\,(ad_m) \qquad \text{Eq. (7)}$$

$$2\,H\,(ad_m) \rightarrow H_2\,(g) + 2\square_m \qquad \text{Eq. (8)}$$

Since there are no phase transitions in kamacite between 400 K and 710 K (Yang *et al.*, 1996), the rate of H_2S dissociation on the metal surface should display Arrhenius kinetic behavior and the reaction rate will increase proportionally with temperature (Worrell, 1971).

The sulfide in equilibrium with kamacite is stoichiometric troilite (FeS) (Ma *et al.*, 1997). Thus, the first metal sulfide molecules form by direct reaction between Fe atoms in kamacite and adsorbed S atoms on the metal surface (Fig. 11a). There are two solid-state phase transitions in FeS that are associated with electromagnetic phenomena (Chase *et al.*, 1985). The FeS phase that forms is therefore temperature dependent. The relevant reactions are:

$$\alpha + S\,(ad_m) \rightarrow \gamma\text{-FeS} + \gamma + \square_s \quad (598\ K \le T \le 710\ K) \qquad \text{Eq. (9)}$$

$$\alpha + S\,(ad_m) \rightarrow \beta\text{-FeS} + \gamma + \square_s \quad (411\ K \le T \le 598\ K) \qquad \text{Eq. (10)}$$

$$\alpha + S\,(ad_m) \rightarrow \alpha\text{-FeS} + \gamma + \square_s \quad (T \le 411\ K) \qquad \text{Eq. (11)}$$

where $\square_s$ refers to a vacant sulfide surface site, α represents kamacite, γ is taenite, and α-, β-, and γ-FeS are the three troilite phases. Thus, the sulfide layers that formed at 558 K are β–FeS, while those that formed at 613 K and 643 K are γ–FeS. Both phases convert to the low-temperature α–FeS upon cooling. Direct reaction between metal and adsorbed S atoms continues until a monolayer of FeS covers the metal surface. Once the metal is shielded from the gas by a layer of troilite, the H_2S molecules adsorb and dissociate on the sulfide surfaces in a series of reactions analogous to Eqs. (5–8). The adsorbed S atoms react with cations that diffuse outward through the sulfide layer. The increase in reaction rate from 613 K to 643 K is related to H_2S dissociation. At 643 K, there is a larger fraction of gas molecules with enough energy to overcome the energy barrier for H_2S dissociation. Therefore, there is relatively more reactive S present on the sulfide surface at 643 K then at 613 K, and the reaction rate increases accordingly.

Troilite formation changes the bulk composition of the remnant metal. The continuous transfer of Fe atoms from metal to the outer edge of the sulfide enriches the remaining metal in Ni (Fig. 11b). Cation diffusion in the metal is orders of magnitude slower than sulfide formation (Million *et al.*, 1981; Dean and Goldstein, 1986). This sluggish diffusion prevents the metal from homogenizing and results in a thin band of taenite at the metal surface (Bastow *et al.*, 1985). The sulfide composition is intimately related to the Ni content of the metal. When the metal in contact with the sulfide layer becomes Ni enriched, Ni-bearing sulfides become stable. The sulfide composition at the metal-sulfide interface is controlled by the metathetical exchange reaction:

$$Fe + NiS = Ni + FeS \qquad \text{Eq. (12)}$$

The activity of NiS can be expressed as:

$$a_{NiS} = \frac{a_{FeS}a_{Ni}}{a_{Fe}} \bullet \frac{1}{K_{12}} \qquad \text{Eq. (13)}$$

where a_i is the activity of species i and K_{12} is the equilibrium constant for Eq. (12). Constant K_{12} is related to temperature through:

$$\log K_{12} = \frac{435.73}{T} + 1.24 \quad (400\ \text{K} < T < 700\ \text{K}) \qquad \text{Eq. (14)}$$

The constants in Eq. (14) are derived from thermodynamic data for NiS (Chase *et al.*, 1985) and FeS (Grønvold and Stølen, 1992). Equations (13) and (14) show that the activity of NiS is a function of the Ni content of the metal and the temperature of reaction. However, the cation% Ni in the sulfide is less than that in the metal. Thus, the formation of Ni-bearing sulfides does not consume the entire band of Ni-enriched metal. Sulfurization at this stage of reaction is expressed as (Fig. 11c):

$$\alpha + H_2S \rightarrow \gamma + (Fe,Ni,Co)_{1-x}S \qquad \text{Eq. (15)}$$

In their study of Fe,Ni sulfurization, Orchard and Young (1989b) observed Ni-rich sulfide nucleation within 40 min at 888 and 938 K and within 8 h at 793 K. Since we observe Ni-bearing sulfides after 24 h of reaction, the time scale for Ni-bearing sulfide nucleation in our experiments is less than one day.

In order to form Ni-bearing sulfides, both Fe and Ni cations diffuse outward through the sulfide layer. The rate of diffusion for Ni^{2+} is at least twice that for Fe^{2+} (Orchard and Young, 1989a; Narita and Nishida, 1975). This difference in diffusion rates results in a Ni content that increases monotonically in the sulfide layer with distance from the metal-sulfide interface (Wagner, 1969). Eventually, the solubility limit for Ni in mss is exceeded and exsolution of pentlandite occurs through:

$$9\,(Fe,Ni,Co)_{1-x_1}S \rightarrow (Fe,Ni,Co)_{1-x_2}S + (Fe,Ni,Co)_{9-x_3}S_8 \qquad \text{Eq. (16)}$$

where x_1 indicates variations in solid solution compositions:

$$x_1 = 1 - \frac{10 - x_2 - x_3}{9}$$

This process is illustrated in Fig. 11d.

Our experimental results suggest that H_2S dissociation is catalyzed on the surface of Ni-rich sulfides. The rapid kinetics observed at 558 K may be due to H_2S dissociation on pentlandite, which is concentrated at the outer edge of the sulfide layers (see Fig. 5). This results in an abundance of reactive S atoms on the sulfide surface. Since S^{2-} diffusion through FeS is extremely slow (Condit *et al.*, 1974), cations must diffuse outward through the sulfide layer and react with the S atoms on the sulfide surface. This results in rapid, parabolic kinetics at 558 K (see Fig. 10) (Schmalzried, 1995).

Young and Orchard (1991) observed a similar phenomenon in the sulfurization kinetics of an Fe-41wt% Ni alloy. They found that when Ni-rich sulfide phases nucleated in their sulfide layers at 793 K, the rate of H_2S dissociation increased drastically. As a result, the reaction behavior switched from linear to steady-state parabolic kinetics and the reaction rate increased dramatically.

Cations are also supplied by diffusion through the sulfide layer at higher temperatures. At both 613 K and 643 K, however, the pentlandite grains are embedded in the interior of the sulfide layers and are not concentrated at the outer sulfide edge (see Figs. 6 and 7). This inhibits the rapid H_2S dissociation that occurs at 558 K, and H_2S dissociation continues to be the rate-limiting mechanism. Eventually, a critical thickness is reached where the rate of cation transport through the sulfide layer is equal to the rate of H_2S dissociation. This results in a transition from linear to parabolic kinetics (see Fig. 10c). The distribution of pentlandite is related to Ni diffusion in the sulfide layers. The difference between the location of pentlandite in the layers that formed at 558 K and those that formed at 613 K and 643 K may be related to the magnetic phase transition at 598 K. However, more work needs to be done to resolve this issue.

Cation diffusion through sulfide layers results in a preferred orientation of the sulfide crystals. This is due to the strong dependence of diffusion rates on crystallographic orientation. Condit *et al.* (1974) showed that Fe^{2+} diffusion in pyrrhotite is most rapid along the *a* axis of the hexagonal unit cell. This means that sulfide crystals oriented with their *a* axes perpendicular to the metal surface rapidly transport cations to the sulfide layer surface and eventually outgrow grains with other orientations. The development of a preferred orientation precedes the onset of parabolic kinetics. Thus, the sulfide layers whose growth follows parabolic kinetics throughout the entire duration of the experiments (558 K) have preferred orientations after very short reaction times (see Fig. 4a). On the other hand, if H_2S dissociation is much slower than cation diffusion (613 K and 643 K), then the sulfide layers will be composed of randomly oriented crystals until the critical sulfide layer thickness is reached and the kinetic behavior changes.

The continuous outward transport of cations causes the metal surface to retreat from the lower edge of the sulfide. This creates a long horizontal gap between the metal and sulfide (Fig. 11d). Lateral stresses imposed by the increase in molar volume resulting from sulfide formation push the sulfide layer down into this gap where it reestablishes contact with the metal. This process continues until the plastic deformation limit of the sulfide is exceeded and the sulfide layer fractures (Fig. 11e). The resulting cracks in the sulfide layer allow the H_2S gas to penetrate directly to the metal surface and form a second, inner sulfide layer. However, the outer edge of the metal is no longer kamacite but has transformed to taenite, which is significantly enriched in Ni, and P. Sulfurization of taenite produces mss and an Ni- and P-rich phase (tentatively identified as barringerite) through the reaction:

$$\gamma(\text{P-enriched}) + H_2S\ (g) \rightarrow (Ni,Fe,Co)_2P + (Fe,Ni,Co)_{1-x}S + H_2\ (g) \qquad \text{Eq. (17)}$$

Formation of the Ni- and P-rich inner layer consumes the entire band of enriched metal (Fig. 11e). Thus, sulfurization does not produce any overall change in the bulk composition of the metal. Instead, Fe, Ni, Co, and P are distributed among three different phases. The inner layer continues to grow until the gap between the metal and sulfide is filled. Once this occurs, chemical communication between the metal and outer sulfide layer is reestablished, and the transport of cations to the outer edge of the sulfide layer resumes. This cycle of gap formation, outer layer disruption, and growth of the inner layer continues throughout the duration of sulfurization. In contrast to Eq. (1), our experimental results suggest the following net reaction for sulfurization of kamacite in a solar composition gas:

$$\underset{\text{(kamacite)}}{\alpha} + H_2S\ (g) \rightarrow \underset{\text{(barringerite)}}{(Ni,Fe,Co)_2P} + \underset{\text{(pentlandite)}}{(Fe,Ni,Co)_{9-x2}S_8} + \underset{\text{(mss)}}{(Fe,Ni,Co)_{1-x3}S} + H_2(g) \qquad \text{Eq. (18)}$$

From the above discussion, it is apparent that both thermodynamic stability and reaction kinetics influence the composition and morphology of the sulfide layers. These relationships are illustrated by a diffusion path, which traces the compositional variation of metal sulfide assemblages on the appropriate ternary phase diagram. The qualitative ternary plots shown in Fig. 11a–d illustrate the evolution of the diffusion path for sulfurization of meteoritic metal. Figure 11e represents the diffusion path in the Fe-Ni-S-P quaternary system projected on the Fe-Ni-S ternary diagram. Furthermore, the path drawn in Fig. 11e is a combination of two diffusion paths. The

second path is a result of the cracking of the outer sulfide layer and subsequent reaction between Ni (and P) rich metal and H_2S gas.

FINGERPRINT OF A NEBULAR SULFIDE

In our previous study of Fe,Ni sulfurization (Lauretta *et al.*, 1996b), we discussed several important elemental fractionations that can help determine whether sulfide assemblages observed in chondrites formed *via* a gas-solid reaction. However, these experiments were done at temperatures and H_2S-H_2 ratios higher than those expected for the solar nebula. The experimental results presented here expand on this work to provide compositions and morphological relationships expected for pristine nebular condensate sulfides. The assemblage resulting from sulfurization of meteoritic metal at low temperature is a solar composition kamacite core surrounded by at least two sulfide layers. The inner layer(s) are composed of a fine-grained mixture of phosphide and sulfide phases. The outer layer(s) contain either fine-grained, randomly oriented mss crystals; blocky, uniformly oriented mss grains; or a combination of the two. Pentlandite inclusions will be dispersed throughout the outer layers. The cation/S ratios and the Ni and P contents of the inner layer will decrease with distance from the metal. The Ni content of the outer layer will increase away from the inner layer. The cation/S ratio in the mss decreases with distance from the metal. The bulk Fe/Ni ratio of the metal and sulfide will be similar. The metal and sulfide layers are typically separated from each other by large gaps. These gaps may allow the sulfide layers to detach from the metal during collisions in the nebula. Thus, the metal and the two types of sulfide layers are likely to be dispersed throughout the matrices of primitive meteorites. In fact, such dispersed nebular sulfide condensates may have already been found in carbonaceous chondrites (Lauretta *et al.*, 1997).

TIME SCALES FOR SULFIDE FORMATION IN THE SOLAR NEBULA

Finally, we apply our experimental results to the rate of sulfide formation in the solar nebula. We use our rate constants to calculate the time scales of metal sulfurization in the solar nebula. The reaction rate is related to the surface area to volume ratio of the metal. We incorporate this dependence by calculating the time required to condense 100% of nebular S as a function of metal grain size. We assumed that metal was uniformly dispersed throughout the solar nebula as spherical grains of equal radii. The amount of S condensed as a function of time is determined by:

$$W_{H_2S} = A_m k_l t \quad \text{(linear kinetics)} \qquad \text{Eq. (19)}$$

$$W_{H_2S} = A_m k_p t^{\frac{1}{2}} \quad \text{(parabolic kinetics)} \qquad \text{Eq. (20)}$$

where W_{H_2S} is the mass of S condensed, A_m is the metal surface area, k_l and k_p are the linear and parabolic practical tarnishing rate constants, and t is time. The lifetimes of metal grains with radii ranging from 0.1 μm to 1 cm are presented in Table 5. Sulfurization is an extremely rapid process and S will be 100% condensed in time scales ranging from ~30 min (0.1 μm radius grains) to ~320 years (1 cm radius grains) at 643 K. These times are slightly higher than our previous estimates (Lauretta *et al.*, 1996a) and are well within the nebular lifetime of 0.1–10 Ma (Podosek and Cassen, 1994). It is possible that the rate-limiting step in the linear kinetic regime changes between the ~1 atm total pressure present in our experiments and the 10^{-3} to 10^{-6} atm in the inner solar nebula (*e.g.*, Fegley and Prinn, 1989). This scenario is discussed in detail in our earlier paper (Lauretta *et al.*, 1996a), where we show that, even under nebular pressures, sulfurization is a rapid process. Thus, we conclude that sulfur condensation *via* metal sulfurization in the solar nebula was not kinetically inhibited.

TABLE 5. Sulfur condensation times in the solar nebula.

Grain radius (cm)	$\log_{10}$ Lifetime (years) 558 K	613 K	643 K
0.00001	–7.6	–4.1	–4.2
0.0001	–5.6	–3.1	–3.2
0.001	–3.6	–2.1	–2.2
0.01	–1.6	–1.3	–1.5
0.1	0.4	0.7	0.5
1	2.4	2.7	2.5

SUMMARY

Kamacite was sulfurized at temperatures and gas compositions relevant to the solar nebula. This resulted in sulfide reaction rims with inner layers composed of a mixture of barringerite ($(Ni,Fe,Co)_2P$) and mss ($(Fe,Ni,Co)_{1-x}S$) and outer layers of uniformly oriented mss grains containing pentlandite ($(Fe,Ni,Co)_{9-x}S_8$) inclusions. The bulk composition of the metal was not significantly altered by the sulfurization process. Application of our experimentally determined reaction rates showed that sulfurization is a rapid process that should have gone to completion well within the lifetime of the solar nebula.

Acknowledgments–This work was supported by NASA grant NAG5-4323 (formerly NAGW-3070). D. S. L. thanks the Barringer Crater Company for providing travel grants that allowed him to attend the Meteoritical Society meetings in 1994 and 1996. We thank the Field Museum in Chicago for providing the samples of Canyon Diablo used in these experiments. We also thank D. Kremser for technical assistance and Y. Hong for helpful discussions. J. I. Goldstein, R. Reisner, and B. Zanda provided constructive reviews.

Editorial handling: J. Goldstein

REFERENCES

ANDERS E. AND GREVESSE N. (1989) Abundances of the elements: Meteoritic and solar. *Geochim. Cosmochim. Acta* **53,** 197–214.

ARMSTRONG J. T. (1988) Quantitative analysis of silicate and oxide minerals: Comparison of Monte-Carlo, ZAF and Phi-Rho-Z procedures. *Microbeam Analysis*, 239–246.

BASTOW B. D., WOOD G. C. AND WHITTLE D. P. (1985) The segregation of alloy components in scales and subscales formed by binary alloys of Mn, Fe, Co and Ni. *Corros. Sci.* **25,** 253–285.

BENNETT M. E., III AND MCSWEEN H. Y., JR. (1996) Shock features of iron-nickel metal and troilite of L-group chondrites. *Meteorit. Planet. Sci.* **31,** 255–264.

CHASE M. W., JR., DAVIES C. A., DOWNEY J. R., JR., FRURIP D. J., MCDONALD R. A. AND SYVERUD A. N. (1985) *JANAF Thermochemical Tables, 3rd edition. J. Phys. Chem. Ref. Data* **14, (Suppl.)** no. 1, Amer. Chem. Soc. and Amer. Inst. of Phys. 1856 pp.

CONDIT R. H., HOBBINS R. R. AND BIRCHENALL C. E. (1974) Self-diffusion of iron and sulfur in ferrous sulfide. *Oxid. Met.* **8,** 409–455.

DEAN D. C. AND GOLDSTEIN J. I. (1986) Determination of the interdiffusion coefficients in the Fe-Ni and Fe-Ni-P systems below 900 °C. *Met. Trans. A* **17A,** 1131–1138.

DREIBUS G., PALME H., SPETTEL B., ZIPFEL J. AND WÄNKE H. (1995) Sulfur and selenium in chondritic meteorites. *Meteoritics* **30,** 439–445.

FEGLEY B., JR. AND LEWIS J. S. (1980) Volatile element chemistry in the solar nebula: Na, K, F, Cl, Br, and P. *Icarus* **41,** 439–455.

FEGLEY B., JR. AND PRINN R. G. (1989) Solar Nebula Chemistry: Implications for Volatiles in the Solar System. In *The Formation and Evolution of Planetary Systems* (eds. H. Weaver and L. Danly), pp. 171–211. Cambridge Univ. Press, Cambridge, U. K.

FRYT E. M., BHIDE V. S., SMELTZER W. W. AND KIRKALDY J. S. (1979) Growth of the iron sulfide ($Fe_{1-\delta}S$) scale on iron at temperatures 600 °–1000 °C. *J. Electrochem. Soc.* **126,** 683–688.

GRØNVOLD F. AND STØLEN S. (1992) Thermodynamics of iron sulfides II. Heat capacity and thermodynamic properties of FeS and of $Fe_{0.875}S$ at temperatures from 298.15 K to 1000 K, of $Fe_{0.98}S$ from 298.15 K to 800 K, and of $Fe_{0.89}S$ from 298.15 K to about 650 K. Thermodynamics of formation. *J. Chem. Thermo.* **24,** 913–936.

GROSSMAN L. AND LARIMER J. W. (1974) Early chemical history of the solar system. *Rev. Geophys. Space Phys.* **12,** 71–101.

HERPFER M. A., LARIMER J. W. AND GOLDSTEIN J. I. (1994) A comparison of metallographic cooling rate methods used in meteorites. *Geochim. Cosmochim. Acta* **58,** 1353–1366.

KELLY W. R. AND LARIMER J. W. (1977) Chemical fractionations in meteorites-VIII. Iron meteorites and the cosmochemical history of the metal phase. *Geochim. Cosmochim. Acta* **41,** 93–111.

KERRIDGE J. F. (1977) Iron: Whence it came, where it went. *Space Sci. Rev.* **20,** 3–68.

KERRIDGE J. F. (1979) Clues to the origin of sulfide minerals in CI chondrites. *Earth Planet. Sci. Lett.* **15,** 286–290.

KREUZER H. J. AND GORTEL Z. W. (1986) *Physisorption Kinetics*. Springer Verlag, Berlin, Germany. 325 pp.

LAURETTA D. S., KREMSER D. T. AND FEGLEY B., JR. (1996a) The rate of iron sulfide formation in the solar nebula. *Icarus* **122,** 288–315.

LAURETTA D. S., KREMSER D. T. AND FEGLEY B., JR. (1996b) A comparative study of experimental and meteoritic metal-sulfide assemblages. *Proc. NIPR Symp. Antarct. Meteorites.* **9,** 97–110.

LAURETTA D. S., LODDERS K. AND FEGLEY B., JR. (1997) Experimental simulations of sulfide formation in the solar nebula. *Science* **277,** 358–360.

LEWIS J. S. (1972) Metal/silicate fractionation in the solar system. *Earth Planet. Sci. Lett.* **43,** 359–367.

LEWIS R. S. AND ANDERS E. (1975) Condensation time of the solar nebula from extinct ^{129}I in primitive meteorites. *Proc. Natl. Acad. Sci. USA* **72,** 268–273.

MA L., WILLIAMS D. B. AND GOLDSTEIN J. I. (1997) Determination of the Fe-rich portion of the Fe-Ni-S phase diagram. *J. Phase Equilibria*, in press.

MCSWEEN H. Y., SEARS D. W. G. AND DODD R. T. (1988) Thermal metamorphism. In *Meteorites and the Early Solar System* (eds. J. F. Kerridge and M. S. Matthews), pp. 102–113. Univ. Arizona Press, Tucson, Arizona, USA.

MILLION B., RUZICKOVA J., VELISEK J. AND VRESTAL J. (1981) Diffusion processes in the Fe-Ni system. *Mat. Sci. Eng.* **50,** 43–52.

NARITA T. AND NISHIDA K. (1975) Kinetics and cation distribution in the ferrous-nickel sulfide scales on iron-nickel alloys. *Denki Kagaku* **43,** 443–451.

NARITA T. AND NISHIDA K. (1976) Cation distributions in the ferrous sulfide scales formed on binary alloys. *Denki Kagaku* **44,** 159–164.

ORCHARD J. P. AND YOUNG D. J. (1989a) Morphological evolution during sulphidation of an iron-nickel alloy. *Oxid. Met.* **31**, 105–121.

ORCHARD J. P. AND YOUNG D. J. (1989b) Sulfidation behavior of an Iron-nickel alloy. *J. Electrochem. Soc.* **136,** 545–550.

PODOSEK F. A. AND CASSEN P. (1994) Theoretical, observational, and isotopic estimates of the lifetime of the solar nebula. *Meteoritics* **29,** 6–25.

RUBIN A. E., FEGLEY B. AND BRETT R. (1988) Oxidation states in chondrites. In *Meteorites and the Early Solar System* (eds. J. F. Kerridge and M. S. Matthews), pp. 488–511. Univ. Arizona Press, Tucson, Arizona, USA.

SCHMALZRIED H. (1995) *Chemical Kinetics of Solids*. VCH Publishers, New York, New York. 433 pp.

SEARS D. W. (1978) Condensation and the composition of iron meteorites. *Earth Planet. Sci. Lett.* **41,** 128–138.

SHEWMAN R. W. AND CLARK L. A. (1970) Pentlandite phase relations in the Fe–Ni-S system and notes on the monosulfide solid solution. *Can. J. Earth Sci.* **7**, 67–85.

SKRZYPEK Z. AND WERBER T. (1976) A kinetic investigation of the sulphurization of iron-nickel alloys in sulphur vapour. *Archiwum Hutnictwa* **21,** 115–124.

STRAFFORD K. N. AND MANIFOLD R. (1969) The corrosion of Fe and some Fe-based alloys in S vapour at 500 °C. *Corros. Sci.* **9,** 489–507.

WAGNER C. (1969) The distribution of cations in metal oxide and metal sulphide solid solutions formed during the oxidation of alloys. *Corros. Sci.* **9,** 91–109.

WERBER T., BIEGUN T., SKRZYPEK Z. AND PODKORODECKI J. (1970) Kinetics of sulphurization of Fe-Ni alloys in sulphur vapours. *Roczniki Chemii* **41,** 915–918.

WORRELL W. L. (1971) Dissociation of gaseous molecules on solids at high temperature. In *Advances in High Temperature Chemistry Vol. 4* (ed. L. Eyring), pp. 71–105. Academic Press, New York, New York, USA.

YANG C. W., WILLIAMS D. B. AND GOLDSTEIN J. I. (1996) A revision of the Fe-Ni phase diagram at low temperatures (<400 °C). *J. Phase Equilibria* **17,** 522–531.

YOUNG D. J. AND ORCHARD J. P. (1991) Surface effects in sulfidation reactions. *Can. Met. Quart.* **30,** 227–233.